

Long-Wavelength Anomalies in the Asymptotic Behavior of Mode-Coupling Theory

S K Schnyder,¹ F Höfling,² T Franosch,³ and
Th Voigtmann^{1,4}

¹Institut für Materialphysik im Weltraum, Deutsches Zentrum für Luft- und Raumfahrt (DLR), 51170 Köln, Germany and Fachbereich Physik, Universität Konstanz, 78457 Konstanz, Germany

²Max-Planck-Institut für Metallforschung, Heisenbergstraße 3, 70569 Stuttgart and Institut für Theoretische und Angewandte Physik, Universität Stuttgart, Pfaffenwaldring 57, 70569 Stuttgart, Germany

³Institut für Theoretische Physik, Universität Erlangen-Nürnberg, Staudtstraße 7, 91058 Erlangen, Germany

⁴Zukunftskolleg, Universität Konstanz, 78457 Konstanz, Germany

Abstract. We discuss the dynamic behavior of a tagged particle close to a classical localization transition in the framework of the mode-coupling theory of the glass transition. Asymptotic results are derived for the order parameter as well as the dynamic correlation functions and the mean-squared displacement close to the transition. The influence of an infrared cutoff is discussed.

PACS numbers: 66.30.hh 61.43.-j 46.65.+g

1. Introduction

Recently, there has been renewed interest in the slow transport of particles in heterogeneous disordered environments, for example, the diffusion in porous media [1–5], or anomalous-diffusion phenomena in binary glass forming mixtures [6–8]. Applications arise in many diverse subjects of science and engineering, notably the physics of transport in crowded biological systems [9], ion transport in glass formers [10, 11], or the geophysics of volcano eruptions [12].

One way of modeling such systems is by binary systems composed of a slowly relaxing “matrix” component and a “fast” species responsible for the transport. This naturally leads to binary mixtures of particles with disparate sizes, be they soft [6] or hard spheres [13, 14]. If the slow matrix is driven to glassy arrest, it forms a random heterogeneous background that can be considered as frozen on the time scale of fast-particle transport. One can also freeze the matrix from the outset, and is led to quenched-annealed mixtures [15–17] or, abstracting even more, the Lorentz gas (LG) model [3–5], a single mobile particle in a random disordered matrix.

All these model systems show intriguing transport phenomena when the matrix is dense enough, although the precise connection for example between the LG model and glass-forming binary mixtures remains to be established [18]. Most notably, the mobile species can undergo a localization transition, where its long-range transport ceases because the embedding matrix is too dense. For the LG, it is understood that

this transition is a dynamic critical phenomenon [19] associated with the percolation of void space between the frozen obstacles. This leads to distinct scaling predictions close to the transition, some of which have only been worked out recently [20].

One of these predictions is anomalous power-law diffusion: the mean-squared displacement (MSD) of the mobile particle, $\delta r^2(t)$, for $t \rightarrow \infty$ does not grow linearly in time as expected for ordinary diffusion. Instead, $\delta r^2(t \rightarrow \infty) \sim t^{2/z}$ with a dynamic critical exponent $z > 2$ is predicted and verified in extensive computer simulations for the LG [3]. In three dimensions, $z = 6.25$ is established, so that $\delta r^2(t \rightarrow \infty) \sim t^{0.32}$. It is not yet clear, whether this asymptotic prediction also holds for a binary mixture, where correlations and residual thermal motion of the background matrix, and the excluded-volume interaction of many tracers come into play [6].

For dense, glass-forming binary mixtures on the other hand, the mode-coupling theory of the glass transition (MCT) [21] provides an excellent theoretical framework that allows many detailed predictions [13, 14, 22]. The glass transition in this framework comes about because of collective local nearest-neighbor caging; quite unlike the single-particle dynamic critical phenomenon that drives the localization transition in the LG model involving a divergent length scale. Connected to this, the glass transition is a discontinuous dynamic transition – the long-time limit (called nonergodicity factor) of the collective dynamic density correlation functions jumps from zero to a nonzero value at the glass transition. In contrast, the localization transition is continuous in this sense and it belongs to a universality class of its own [23]. Theories along the lines of the current MCT have been applied to the LG previously [24–26], and the appearance of continuous transitions in MCT applied to both quenched-annealed [15–17] and size-disparate mixtures [13, 14] cast new attention to the description of such divergent-length localization transitions within that theory.

Most previous studies of localization transitions within MCT have put the influence of a divergent length scale on the theory’s vertex out of focus, explicitly dropping dependencies on wave number q – in the memory kernel only [24], or fully in the form of a schematic model [27] – or by silently introducing small- q cutoffs through numerical discretization. In fact, such a cutoff can be argued for since the small- q structure of MCT’s vertex is incorrect at least in the LG [28]. However, it seems to be largely undocumented so far how sensitive the expected results are to such a cutoff.

Here we document the dependence of asymptotic results of MCT close to localization transitions on the small-wave-number regime. The analytic results are corroborated by careful numerical evaluation of the MCT integrals for the tagged-particle correlators. We identify the regime where the solutions are dominated by the small- q features by studying the dependence of the solutions on an ad-hoc infrared cutoff. For simplicity, we obtain numerical solutions for the LG model, but the generic picture is the same in the MCT for mixtures or quenched-annealed systems.

2. Methods

Consider a mixture of classical hard-sphere particles in d dimensions, with diameters d_α , where Greek indices label the different species. $N = \sum_\alpha N_\alpha$ is the total number of particles in a box of volume V , by $x_\alpha = N_\alpha/V$ we denote the respective number concentrations. Since we are interested in single-particle transport quantities, we consider the dynamic tagged-particle density correlation function,

$$\phi_\alpha(q, t) = \langle \varrho_\alpha^{s*}(\vec{q}, t) \varrho_\alpha^s(\vec{q}) \rangle, \quad (1)$$

where $\varrho_\alpha^s(\vec{q}, t) = \exp[i\vec{q} \cdot \vec{r}_{\alpha,s}(t)]$ is the corresponding tagged-particle density fluctuation to wave vector \vec{q} , and $\vec{r}_{\alpha,s}(t)$ the trajectory of the singled-out tracer particle (taken to be of species α). $\phi_\alpha(q, t)$ is real-valued and does not depend on the direction of the wave vector \vec{q} for a translational-invariant and isotropic system; we also omit the $t = 0$ argument since we assume all dynamics to be time-translational invariant. For convenience, it serves to introduce the Laplace transformed $\phi_\alpha(q, z) = i \int_0^\infty e^{izt} \phi_\alpha(q, t) dt$ for complex frequency z such that the integral converges.

Starting from Newton's equations of motion, the time evolution of the tagged-particle correlation function can be represented by a Mori-Zwanzig equation [21],

$$\phi_\alpha(q, z) = - \left[z - \frac{q^2}{z/v_{\text{th},\alpha}^2 + i\nu_\alpha q^2 + m_\alpha(q, z)} \right]^{-1}, \quad (2)$$

where $v_{\text{th},\alpha} = \sqrt{k_B T/m_\alpha}$ is the thermal velocity of the particles with mass m_α , characterizing the ballistic short-time motion. The term $\nu_\alpha = \sqrt{\pi} \varrho v_{\text{th},\alpha} \sum_\beta x_\beta g_{\alpha\beta} R_{\alpha\beta}^2 \sqrt{2\mu_{\alpha\beta}}$ arises because for hard spheres, the dynamics is described by a non-self-adjoint pseudo-Liouville operator [29], and is a central quantity calculated in Enskog theory [30, 31]. For brevity, we have set $R_{\alpha\beta} = d_\alpha + d_\beta$ and $\mu_{\alpha\beta} = m_\beta/(m_\alpha + m_\beta)$, and denoted by $g_{\alpha\beta}$ the value of the radial distribution function for two particles of species α and β at contact. In the time domain, Eq. (2) reads

$$\begin{aligned} \frac{1}{v_{\text{th},\alpha}^2} \partial_t^2 \phi_\alpha(q, t) + q^2 \nu_\alpha \partial_t \phi_\alpha(q, t) + q^2 \phi_\alpha(q, t) \\ + \int_0^t m_\alpha(q, t-t') \partial_{t'} \phi_\alpha(q, t') dt' = 0, \end{aligned} \quad (3)$$

with initial conditions $\phi_\alpha(q, 0) = 1$ and $\dot{\phi}_\alpha(q, 0) = 0$. We are not interested in the short-time dynamics. Therefore, numerical solutions are later shown for the overdamped case, where the second derivative in Eq. (3) and thus inertia terms are dropped. We can then set $\nu_\alpha = 1$ to define the unit of time. For the resulting Brownian dynamics, the low-density asymptote of the LG has been worked out exactly [32].

The memory kernel $m_\alpha(q, t)$ is formally given as a correlation function of generalized fluctuating forces. MCT assumes the dominant contribution in the relaxation of these forces to be given by their overlap with density-pair fluctuations – for the tagged-particle dynamics, with pair modes of the form $\varrho_\beta^s(\vec{k}, t) \varrho_\gamma(\vec{p}, t)$, formed with the collective number-density fluctuations $\varrho_\alpha(\vec{q}, t) = \sum_{k=1}^{N_\alpha} \exp[i\vec{q} \cdot \vec{r}_{\alpha,k}(t)]$, where $\vec{r}_{\alpha,k}(t)$ is the trajectory of the k -th particle of species α . The corresponding collective partial number density correlation functions are denoted by $\Phi_{\alpha\beta}(q, t) = \langle \varrho_\alpha^*(\vec{q}, t) \varrho_\beta(\vec{q}) \rangle$, and their initial value is the static structure factor, $\mathbf{S}(q) = \Phi(q, 0)$. The MCT expression for the tagged-particle memory kernel then reads

$$m_\alpha(q, t) \approx \varrho \int \frac{d^d k}{(2\pi)^d} (\vec{e}_{\vec{q}} \vec{k})^2 c_{\alpha\alpha'}(k) c_{\alpha\alpha''}(k) \Phi_{\alpha'\alpha''}(k, t) \phi_\alpha(p, t). \quad (4)$$

where ϱ is the total number density of the d -dimensional system. It is hence expressed as a bilinear functional of the tagged-particle density correlation function $\phi_\alpha(p, t)$, and of the collective density correlators $\Phi_{\alpha\beta}(k, t)$. Momentum conservation implies $\vec{q} = \vec{k} + \vec{p}$, and we denote by $\vec{e}_{\vec{q}}$ the unit vector in \vec{q} -direction. The coupling coefficients are given in terms of the Ornstein-Zernike direct correlation functions $c_{\alpha\beta}(q)$.

To determine the full dynamics of the system, one would first need to calculate the collective dynamics, $\Phi(q, t)$, for which analogous MCT expressions can be derived.

In this paper, we are only concerned with the tagged-particle dynamics, in the case where the slow relaxation time of the heterogeneous matrix, $\tau_{\alpha\beta}$, is much larger than the time scales characterizing the nontrivial dynamics of the tracer. We are also interested in slow dynamics beyond the initial short-time transient, i.e., in times $1/\nu_\alpha \ll t \ll \tau_{\alpha\beta}$. In this case, $\Phi(q, t) \approx \mathbf{F}(q) \succ \mathbf{0}$, a positive-definite non-vanishing matrix of nonergodicity factors [33]. It is standard MCT procedure to calculate $\mathbf{F}(q)$ from the given static structure factor of the system. Generically, $\mathbf{F}(q)$ decays at large q to provide an implicit large- q cutoff of the integrals; it is also non-singular at all q .

$$v(k) = \sum_{\alpha\beta\gamma} c_{\alpha\beta}(k)c_{\alpha\gamma}(k)F_{\beta\gamma}(k) > 0 \quad (5)$$

is the effective coupling coefficient that is positive and non-singular. The expression of the MCT memory kernel then reads

$$m_\alpha(q, t) = \varrho \int \frac{d^d k}{(2\pi)^d} (\vec{e}_q \vec{k})^2 v(k) \phi_\alpha(p, t). \quad (6)$$

Rewriting the integral in terms of bispherical coordinates, i.e., in terms of moduli k and p , one realizes that the k -integral can be carried out immediately, and one is left with a linear functional

$$m_\alpha(q, t) \equiv m[\phi](q, t) = \varrho \int dp \tilde{v}_{qp} \phi_\alpha(p, t), \quad (7)$$

where we omit the subscript labeling the species for brevity.

The theory given by Eqs. (3) and (6) is a special case of MCT for the dynamics of a tagged particle in a mixture. In the presence of quenched rather than self-generated disorder, the derivation of such a theory becomes more subtle [16]. Nevertheless, the resulting tagged-particle equations are structurally equivalent [17], as is the MCT for the LG, and also the limit of MCT considering the remaining dynamics of particles deep inside the glass, the strong-coupling limit [34]. To simplify the further numerical procedure, we consider the LG model from now on, i.e., a point tracer among randomly placed (overlapping) hard-sphere obstacles with radius R . The vertex $v(k)$ can then be evaluated explicitly; in $d = 3$ one obtains

$$v_{\text{LG}}(k) = 4(2\pi)^2 R^4 (j_1(kR))^2 > 0, \quad (8)$$

with j_1 the first modified spherical Bessel function. Also, $\nu = \sqrt{\pi} \varrho R^2 v_{\text{th}}$ in this case.

The nonergodicity parameter $f(q) = \lim_{t \rightarrow \infty} \phi(q, t)$ can be determined [33, 35] as the largest positive solution of

$$\frac{f(q)}{1 - f(q)} = m[f](q)/q^2. \quad (9)$$

It is well known that bifurcations exist in these equations: smooth changes of the coupling coefficients (such as induced by a smooth increase in density without structural changes) can lead to singular changes in $f(q)$. Standard MCT considers m to be a nonlinear functional of the f , giving rise to so-called \mathcal{A}_ℓ bifurcations (as classified by Arnol'd) that one identifies as ideal glass transitions where $m(q)$ jumps to a finite value $m^c(q) > 0$ [21]. In the present context, we are concerned with continuous transitions, viz. the critical points in parameter space, where the trivial solution, $f(q) = 0$ for all finite q , changes continuously to a non-trivial solutions $f(q) \geq 0$. At the critical point, $f^c(q) = 0$ for all finite q , and consequently $m^c(q) = 0$ there. Note that for $q = 0$, $f(0) = 1$ holds always. These continuous transitions arise in the LG upon changing the scatterer density ϱ , and in binary-mixture systems through

tuning the parameters such that the combination of direct correlation functions and nonergodicity parameters entering $v(k)$ leads to sufficiently weak coupling.

Not all continuous MCT transitions are of the localization-transition type discussed here. For example, in dumbbell-shaped molecules with top-down symmetry, a glass may form where the rotational degrees of freedom associated with this symmetry remain ergodic, and eventually freeze by further compression [36–41]. This MCT transition is continuous but does not involve a divergent static length scale.

If $m[f]$ is a linear functional as in Eq. (7), we can express f via Eq. (9) to get

$$\begin{aligned} m(q) &= \varrho \int dp \tilde{v}_{qp} \frac{m(p)}{p^2 + m(p)} \\ &= \varrho \int dp W_{qp} m(p) - \varrho \int dp W_{qp} \frac{m(p)^2}{p^2 + m(p)}. \end{aligned} \quad (10)$$

a closed nonlinear integral equation for $m(q)$, where we have introduced $W_{qp} = \tilde{v}_{qp}/p^2$. Expressing m in this form, one recognizes immediately that, whenever m^c is zero for finite k , the peculiarities of the integral at small k become important since there is a dangerous denominator. In the following, we will present both analytical considerations valid asymptotically close to the transition, and numerical results. The latter have been obtained by a specially devised numerical grid for the discretization of integrals like in Eq. (10), described in Appendix A.

3. Results

3.1. Statics

It will be of further importance to understand the small-wave-number limits of the vertex W_{qp} . This depends on the dimensionality; for $d = 3$ one obtains from Eq. (6)

$$W_{qp} = \frac{1}{(2\pi)^2} \frac{1}{4q^3 p} \int_{|q-p|}^{q+p} k dk (q^2 - p^2 + k^2)^2 v(k). \quad (11)$$

Considering $p \rightarrow 0$ at fixed q , $(2\pi)^2 W_{qp} = 2q^2 v(q) + \mathcal{O}(p^2)$, and for $q \rightarrow 0$ at fixed p , $(2\pi)^2 W_{qp} = \frac{2}{3} p v(p) + \mathcal{O}(q^2)$. Thus, W_{qp} is regular in the $q \rightarrow 0$ and $p \rightarrow 0$ limits, and falls off quickly enough at large p to ensure the finiteness of the integrals we consider.

The influence of the small-wavenumber regime in Eq. (10) is easiest understood by introducing an infrared cutoff parameter δ in the integral and discussing the asymptotic dependence on it. Close to the transition, $m(q)$ is small; Eq. (10) becomes a linear integral equation with positive definite kernel W_{qp} . Nontrivial solutions only exist if ϱ is an eigenvalue [42]. The equivalent of the Perron-Frobenius theorem for nonnegative matrices holds, called Jentzsch's theorem in the context of Fredholm integral equations [43]: there exists a non-degenerate minimal eigenvalue ϱ_c that is positive and real, and the corresponding eigenfunction can be chosen real and positive. Obviously, ϱ_c defines the critical density: for densities below, only the trivial solution $m_\delta(q) = 0$ exists, so that the particle is delocalized. We denote the critical eigenfunction by $h(q)$,

$$h_\delta(q) = \varrho_c \int_\delta^\infty dp W_{qp} h_\delta(p). \quad (12)$$

We will also need the eigenfunction $\hat{h}(q)$ of the transposed equation,

$$\hat{h}_\delta(p) = \varrho_c \int_\delta^\infty dq \hat{h}_\delta(q) W_{qp}. \quad (13)$$

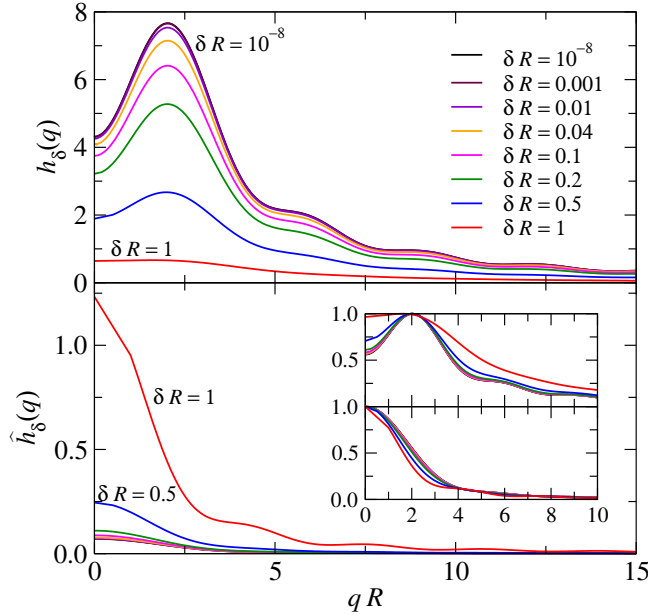


Figure 1. Critical eigenfunctions $h_\delta(q)$ (upper panel) and $\hat{h}_\delta(q)$ (lower panel) for the Lorentz-gas MCT vertex for various δ as indicated, normalized according to Eqs. (14). The functions have been analytically extended to $q < \delta$. The insets show $h_\delta(q)$ and $\hat{h}_\delta(q)$ normalized to their respective maxima.

In order to normalize the eigenfunctions we can impose two conditions, which we choose for later convenience,

$$\int_\delta^\infty dq \hat{h}_\delta(q) h_\delta(q) = 1, \quad \hat{h}_\delta(\delta) h_\delta(\delta)^{3/2} (\pi/2) = 1. \quad (14)$$

Critical eigenfunctions $h_\delta(q)$ and $\hat{h}_\delta(q)$ are shown in Fig. 1 for various cutoff values δ , evaluated for the Lorentz-Gas vertex. Apart from the normalization, the shape of these functions depends rather insensitively on δ , as exhibited by the insets of Fig. 1.

The next-to-leading order expansion of Eq. (10) depends rather more sensitively on δ . We shall distinguish “large” cutoff, $\delta \gg \sqrt{m(\delta)}$, from “small” ones, $\delta \ll \sqrt{m(\delta)}$. In the former case, the term $m(p)$ in the denominator of the second part of Eq. (10) is not relevant close to the transition, and the corresponding integral yields a term of $\mathcal{O}(m^2)$. We thus expand for $\varrho > \varrho_c$

$$m(q) = \sigma h_\delta(q) + \sigma^2 K_\delta(q) + \mathcal{O}(\sigma^3), \quad \delta \text{ large}, \quad (15)$$

where σ is a small parameter quantifying the distance to the transition point in a way to be specified. Introducing $\varepsilon = (\varrho - \varrho_c)/\varrho_c$ and inserting into Eq. (10) we get after multiplication with $\hat{h}_\delta(q)$ and integration over q the solubility condition

$$\sigma = \varepsilon \left(\int_\delta^\infty dq \hat{h}_\delta(q) (h_\delta(q)/q)^2 \right)^{-1} \approx \varepsilon \delta / (\hat{h}_\delta(\delta) h_\delta^2(\delta)), \quad \delta \text{ large}, \quad (16)$$

where in the approximation we have exploited that the integral is dominated by contributions from $q \approx \delta$. In other words, $\sigma \sim \varepsilon$, which is the asymptotic relation also known from the schematic model [27].

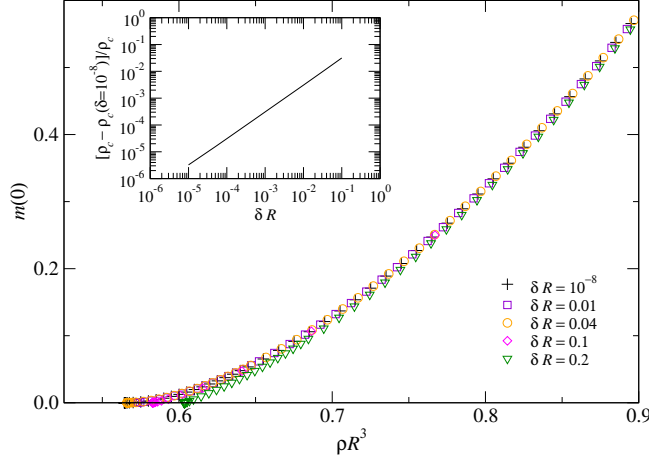


Figure 2. Order parameter $m(0)$ as a function of density ϱ , for various δ as indicated. The inset shows the variation of the critical point, ϱ_c , with δ .

For small cutoff, $\delta \ll \sqrt{m_\delta(\delta)}$, the second part in Eq. (10) needs to be treated with care. Specifically, in the small- p region we can replace $W_{qp} \approx W_{q\delta}$ and $m_\delta(p) \approx m_\delta(\delta)$ in order to perform this part of the integral explicitly. Omitting the remaining terms of $\mathcal{O}(m^2)$, we arrive at

$$m(p) = \varrho \int_\delta^\infty dp W_{qp} m(p) - \varrho W_{q\delta} m^{3/2}(\delta) \frac{\pi}{2} + \mathcal{O}(m^2). \quad (17)$$

We now need to expand differently. Again for $\varrho > \varrho_c$,

$$m(q) = \sigma h_\delta(q) + \sigma^{3/2} \tilde{K}_\delta(q) + \mathcal{O}(\sigma^2), \quad \delta \text{ small}. \quad (18)$$

Inserting this into Eq. (17) and collecting terms of $\mathcal{O}(\sigma^{3/2})$, we obtain

$$\tilde{K}_\delta(q) = \varrho_c \int dp W_{qp} \tilde{K}_\delta(p) \quad (19)$$

$$+ \sigma^{-1/2} \varepsilon \varrho_c \int dp W_{qp} h_\delta(p) - \varrho_c W_{q\delta} h_\delta^{3/2}(\delta) (\pi/2), \quad (20)$$

if we set $\varepsilon \sim \sigma^{1/2}$. The solubility condition is again obtained by contracting with $\hat{h}_\delta(q)$ and reads

$$\sqrt{|\sigma|} = |\varepsilon| / \hat{h}_\delta(\delta) h_\delta(\delta)^{3/2} (\pi/2), \quad \delta \text{ small}, \quad (21)$$

where it is understood that $\varepsilon \geq 0$ corresponds to $\sigma \geq 0$ and denotes the localized respective delocalized side of the transition.

Thus, the asymptotic behavior of $m_\delta(q)$ changes depending on δ . Stated differently, for any fixed infrared cutoff there exist regimes close to the transition where the “large- δ ” asymptote is reached. For distances ε larger than a cross-over distance, the “small- δ ” asymptote holds. We estimate this cross-over by equating the leading-order terms, from which one gets

$$\varepsilon^* = \frac{\hat{h}_\delta(\delta)^2 h_\delta(\delta)^3 (\pi/2)^2}{\int_\delta^\infty dq \hat{h}_\delta(q) h_\delta(q)^2 / q^2} \approx \hat{h}_\delta(\delta) h_\delta(\delta) (\pi/2)^2 \delta. \quad (22)$$

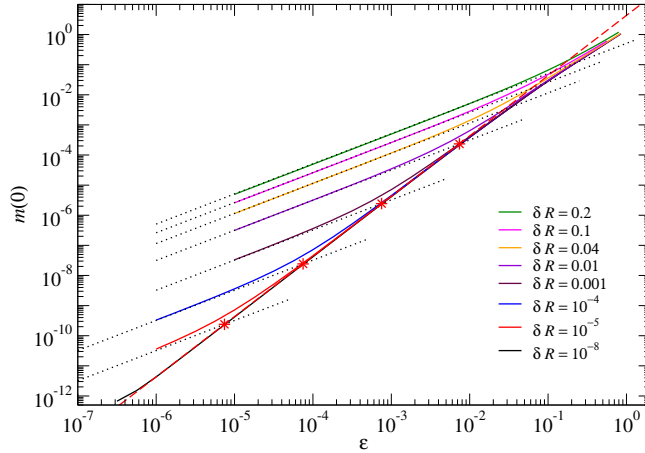


Figure 3. Same as Fig. 2, but plotted double-logarithmically as a function of the distance to the transition $\varepsilon = (\varrho - \varrho_c)/\varrho_c$.

To demonstrate this behavior, let us investigate the order parameter $m(0)$ as a function of density. Numerical results are shown in Fig. 2. Except in a region of densities around 0.6, the curves depend relatively weakly on δ , indicating that the theory in $d = 3$ is for this aspect not sensitive to an infrared cutoff sufficiently far in the localized region. A numerical determination of the critical eigenvalue in Eq. (12) for the LG vertex gives $\varrho_c \approx 0.5644/R^3$ for $\delta \rightarrow 0$. As the inset of Fig. 2 demonstrates, for the $d = 3$ LG vertex, the variation of ϱ_c with δ is small. The localization point found in simulations of the three-dimensional Lorentz gas is $\varrho_c \approx 0.84/R^3$ [3, 5]. It is well known that MCT over-estimates the tendency to arrest, so that we will not be concerned by this discrepancy. Note that a generalized hydrodynamic approach, replacing all occurrences of the memory kernel in Eq. (10) by its $q \rightarrow 0$ limit, allows to directly evaluate the integral using Eq. (8) [24], resulting in $\varrho_c = 9/(4\pi R^3) \approx 0.716R^{-3}$.

The different asymptotic regimes are exhibited in Fig. 3, where $m(0)$ is shown as a function of ε in double-logarithmic fashion. The asymptotes, Eq. (15) together with Eq. (16), and Eq. (18) with Eq. (21), are shown as dotted lines. They are found to agree well with the numerical results. Stars in Fig. 3 mark the cross-over point ε^* , Eq. (22), where the two asymptotic regimes meet.

Figure 4 shows the nonergodicity parameters $f(q)$ obtained for $\delta = 10^{-8}$ and $\delta = 0.01$ for various ε . Inserting the leading-order result $m(q) = |\sigma|h_\delta(q)$ into Eq. (9), we get for $\sigma > 0$

$$f(q) \sim \frac{1}{1 + q^2/(\sigma h_\delta(q))}, \quad (23)$$

so that for small q , $f(q)$ becomes a Lorentzian from which we read off a length scale diverging as $\sim \sigma^{-1/2}$.

3.2. Dynamical Scaling Functions

We are now interested in the dynamic scaling of correlation functions in the limit of large times, i.e., time scales much longer than that of binary collisions. We shall thus

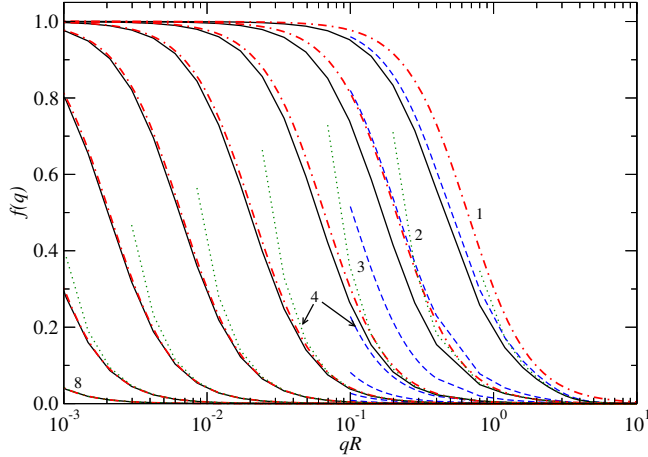


Figure 4. Nonergodicity parameter $f(q)$ corresponding to $\delta = 10^{-8}$ (solid lines) and $\delta = 0.01$ (dashed lines), for $\varepsilon = 10^{-n/2}$ as labeled. The asymptotic results given $m(q)/q^2$ and Eq. (23) are shown in dotted and dash-dotted.

analyze Eq. (2) in the limit $|z| \ll \nu$. Analogously to Eq. (10), we get

$$zm(q, z) = \varrho \int_{\delta}^{\infty} dp W_{qp} z \mu(p, z) + \varrho \int_{\delta}^{\infty} dp W_{qp} \frac{(z\mu(p, z))^2}{p^2 - z\mu(p, z)}, \quad (24)$$

where $z\mu(p, z) = z^2/v_{\text{th}}^2 + p^2 i\nu z + zm(p, z)$. Note in passing that the emerging integrals are well-defined if one assumes $\phi(q, t)$ and $m(q, t)$ to be completely monotone functions. In particular, there then holds for the real part $\Re m(q, z) \geq 0$ for $\Re z < 0$ [44], ensuring the analog of Eq. (17) with m replaced by μ on the r.h.s. One readily obtains that in leading order at the critical point, $m(q, z)$ solves the eigenvalue equation (12) as $z \rightarrow 0$. Thus, $m(q, z) = h_{\delta}(q)G(z) + \delta m(q, z)$. The scaling ansatz observing $m(q) \sim \mathcal{O}(|\sigma|)$ sets $G(z) = |\sigma| t_{\sigma} g(\hat{z})$ for rescaled frequencies $\hat{z} = z t_{\sigma}$. Here t_{σ} is a time scale that diverges faster than $1/|\sigma|$ as the transition is approached. The leading-order term is reminiscent of the standard MCT factorization theorem [21]: wave-number- and frequency-dependence factorize. For the correlator this implies $\phi(q, t) \sim (h(q)/q^2)G(t)$ as $\sigma \rightarrow 0$. But since $\phi(q, t) \leq 1$, at the localization transition the factorization theorem for $\phi(q, t)$ is violated even as $t \rightarrow \infty$ for small q . This is demonstrated in Fig. 4, where dotted lines show $f(q) \sim \sigma h(q)/q^2 \sim m(q)/q^2$.

To obtain the scaling equation, we need to consider the next-to-leading terms and hence distinguish again between small and large δ . In the latter regime, we set, in generalization of Eq. (15),

$$m(q, z) = |\sigma| t_{\sigma} h_{\delta}(q) g(\hat{z}) + \sigma^2 t_{\sigma} \hat{K}(q, \hat{z}) + \mathcal{O}(|\sigma|^3), \quad \delta \text{ large.} \quad (25)$$

Inserting into Eq. (24) and balancing the terms of $\mathcal{O}(\sigma^2)$ yields, after contraction with the left-eigenfunction $\hat{h}_{\delta}(q)$, the scaling equation $i(\tau/t_{\sigma})\hat{z} + \varepsilon|\sigma|\hat{z}g(\hat{z}) + \varepsilon\sigma(\hat{z}g(\hat{z}))^2 = 0$. Here we have used Eqs. (14) and (16) and defined $\tau = \nu \int dp \hat{h}_{\delta}(p)p^2$. We thus fix

$$t_{\sigma} = \frac{\tau}{|\varepsilon||\sigma|}, \quad (26)$$

and get the two scaling solutions for $\sigma \gtrsim 0$,

$$0 = \pm i + g_{\pm}(\hat{z}) \pm \hat{z}(g_{\pm}(\hat{z}))^2, \quad \delta \text{ large.} \quad (27)$$

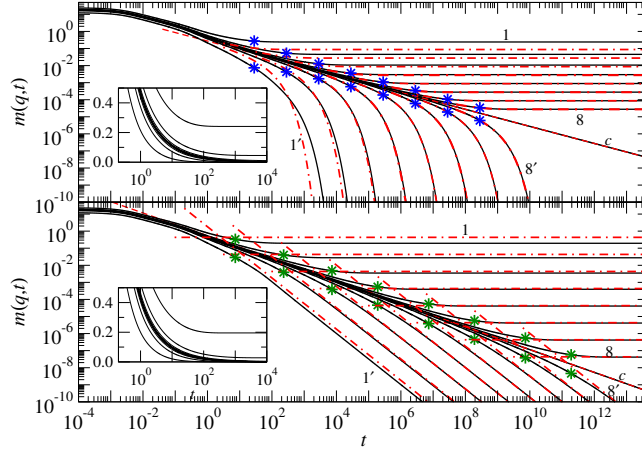


Figure 5. Memory kernel $m(q, t)$ at $q = \delta$, for the case of large δ (top panel) and small δ (bottom panel), for distances to the respective transition points $\varepsilon = \pm 10^{-n/2}$ ($n = 1, \dots, 8$) and $\varepsilon = 0$ (curves labeled c). The asymptotic results obtained from the scaling equations, Eqs. (27) and (31), are shown as dash-dotted lines. Stars mark the time scales t_σ used in the scaling equation. Insets: $m(q, t)$ on a linear-log scale.

This is the scaling equation derived earlier by Götze for the F1 model [21]. Its solution can be given as a closed expression for the inverse Laplace transform, $g(\hat{t})$, where $\hat{t} = t/t_\sigma$. Here we are only interested in the asymptotes. Letting $\hat{z} \rightarrow 0$, we find $g_+(\hat{z}) \sim 1/\hat{z}$. Thus, $g_+(\hat{t}) \rightarrow 1$ for $\varepsilon > 0$, i.e., the signature of localized dynamics. On the other hand $g_-(\hat{z})$ remains regular, indicating that $g_-(\hat{t})$ decays faster than $1/\hat{t}$ at long times (exponential in fact). Letting $\hat{z} \rightarrow \infty$ we obtain $g(\hat{t}) \sim (\pi\hat{t})^{-1/2}$, so that for the time window $1/\nu \ll t \ll t_\sigma$, we have the σ -independent asymptote

$$m(q, t) \sim |\sigma| \frac{h_\delta(q)}{\sqrt{\pi}} \left(\frac{t}{t_\sigma} \right)^{-1/2} \sim \frac{\delta}{\sqrt{\pi h_\delta(\delta)}} \left(\frac{t}{\tau} \right)^{-1/2}, \quad \delta \text{ large.} \quad (28)$$

Note that an explicit dependence on the cutoff parameter remains in the prefactor. The top panel of Fig. 5 exemplifies $m(q = \delta, t)$ in the large- δ regime for various distances ε to the transition. Dash-dotted lines indicate the above asymptotes.

Along similar lines, we deduce the small- δ scaling function. Here we have to expand as in Eq. (18),

$$m(q, z) = |\sigma| t_\sigma h_\delta(q) g(\hat{z}) + |\sigma|^{3/2} t_\sigma \tilde{K}(q, \hat{z}), \quad \delta \text{ small.} \quad (29)$$

Balancing the $|\sigma|^{3/2}$ terms in Eq. (24) we obtain after multiplying with $\hat{h}_\delta(q)$ and integration over q

$$i(\tau/t_\sigma)\hat{z} + \varepsilon|\sigma|\hat{z}g(\hat{z}) + \hat{h}_\delta(\delta)h_\delta(\delta)^{3/2}(\pi/2)|\sigma|^{3/2}(\hat{z}g(\hat{z}))^{3/2} = 0. \quad (30)$$

Now, using Eqs. (21) and (26), this yields for $\varepsilon \geq 0$

$$0 = \hat{z}(g_\pm(\hat{z}))^3 + (g_\pm(\hat{z}))^2 \pm 2ig_\pm(\hat{z}) - 1, \quad \delta \text{ small.} \quad (31)$$

As $\hat{z} \rightarrow \infty$, this equation is solved by $g_\pm(\hat{z}) = i(i\hat{z})^{-1/3}$, and thus $g_\pm(\hat{t}) \sim \hat{t}^{-2/3}/\Gamma(1/3)$ for $1/\nu \ll t \ll t_\sigma$. As $\hat{z} \rightarrow 0$, we note again $g_+(\hat{z}) \sim -1/\hat{z}$ (localized solution), but $g_-(\hat{z}) \sim i - \sqrt{i\hat{z}}$ leading to $g_-(\hat{t}) \sim \hat{t}^{-3/2}/\sqrt{4\pi}$. The behavior we find is thus

$$m(q, t) \sim (\hat{h}_\delta(\delta)\pi/2)^{-2/3}/\Gamma(1/3) (t/\tau)^{-2/3}, \quad t \ll t_\sigma, \delta \text{ small,} \quad (32)$$

$$m(q, t) \sim |\sigma|h_\delta(q)/\sqrt{4\pi} (t/t_\sigma)^{-3/2}, \quad t \gg t_\sigma, \varepsilon \rightarrow 0^-, \delta \text{ small.} \quad (33)$$

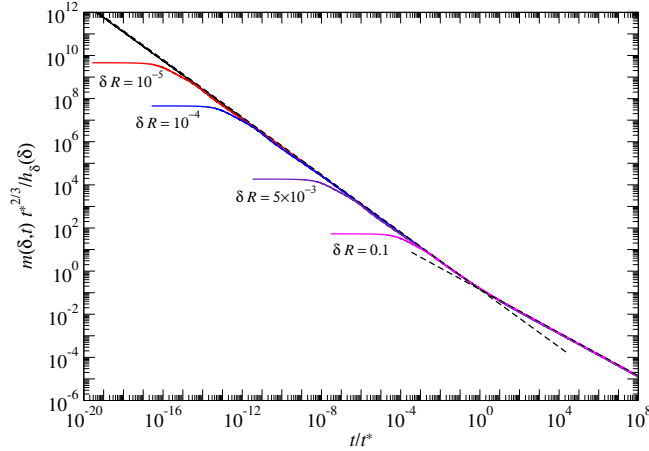


Figure 6. $m(\delta, t)$ at the critical point as a function of t/t^* according to Eq. (34), for various δ as indicated. For the unlabeled curve, $\delta = 10^{-8}/R$.

These power laws are exemplified in the lower panel of Fig. 5, for various ε in the small- δ regime. As for the large- δ regime (upper panel), the asymptotic results describe the numerical solution for $m(q, t)$ well even for $\varepsilon = \mathcal{O}(0.1)$. Treating the small-wavenumber regime of the vertex seriously, a long-time tail for $m(q, t)$ results; however, this is not the known universal long-time tail of the LG [32, 45] in $d = 3$, $t^{-5/2}$, which is not contained in the present MCT.

The two regimes outlined above, large and small δ are separated by the condition $\delta \sim \sqrt{|zm(\delta, z)|}$. For fixed δ , this implies a time scale t^* where the small- δ asymptotics for $t \ll t^*$ crosses over to the large- δ asymptotics for $t \gg t^*$. Equating Eqs. (28) and (32), and using the approximation Eq. (22), we find

$$t^* \approx \frac{16}{\pi \Gamma(1/3)^6 \hat{h}_\delta(\delta)} \frac{\tau}{\delta^3}. \quad (34)$$

Thus, plotting $m(\delta, t)$ at various δ as a function of $\bar{t} = t/t^*$ reveals a master curve with asymptotes $\bar{t}^{-2/3}$ for $\bar{t} \ll 1$, and $\bar{t}^{-1/2}$ for $\bar{t} \gg 1$, for $\sigma \rightarrow 0$; see Fig. 6.

If the cutoff is held fixed, the time scale t_σ marks the cross-over between the different power-law regimes. The small- δ asymptotes are always encountered first, and if the corresponding $t_\sigma < t^*$, the cutoff-influenced large- δ asymptote is not seen. Only close enough to the transition does the cutoff-dependent small- δ asymptote become evident for long times. This can be seen in Fig. 7, where a star marks t^* , and dashed and dash-dotted lines the different asymptotic solutions.

3.3. Mean-Squared Displacement

The mean-squared displacement $\delta r^2(t)$ is obtained from the $q \rightarrow 0$ limit of the correlator, $\phi(q, t) = 1 - (q^2/6)\delta r^2(t)$. Inserting into Eq. (3), one gets after Laplace-transforming the equivalent of Eq. (2),

$$\delta r^2(z) = \frac{1}{z^2} \frac{6v_{\text{th}}^2}{z + i\nu + m(0, z)} \sim \frac{6v_{\text{th}}^2}{|\sigma|h_\delta(0)t_\sigma} \frac{1}{\hat{z}^2 g(\hat{z})}. \quad (35)$$

The latter asymptotic behavior is seen from inserting the leading-order result for $m(0, z)$ and noticing that $t_\sigma \rightarrow \infty$ close to the transition. The generic features of

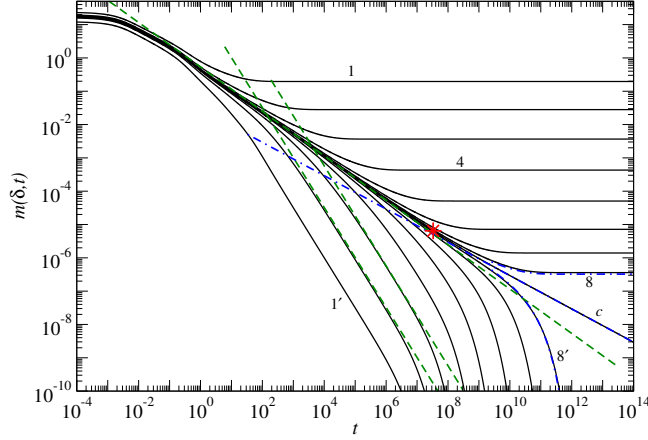


Figure 7. $m(\delta, t)$ as a function of t , for $\delta = 10^{-3}$, at various distances to the transition, $\varepsilon = \pm 10^{-n/2}$ as labeled and $\varepsilon = 0$ (label c). Dashed lines show small- δ asymptotes, dash-dotted lines the large- δ asymptotes at the critical point and for exemplary ε . A star marks t^* , Eq. (34).

$\delta r^2(t)$ at long times are then immediately clear from those of $m(0, t)$. For $\varepsilon > 0$, from $g(\hat{z}) \sim -1/\hat{z}$ there results the localization length

$$r_c = \sqrt{\delta r^2(\infty)/6} = \frac{v_{\text{th}}}{|\sigma|^{1/2} h_\delta^{1/2}(0)}, \quad \varepsilon > 0. \quad (36)$$

On the liquid side, $g_-(\hat{z})$ remains regular as $\hat{z} \rightarrow 0$. We then get ordinary diffusion,

$$\delta r^2(t \rightarrow \infty) \sim \frac{6v_{\text{th}}^2}{|\sigma| h_\delta(0)} \frac{t}{t_\sigma}, \quad \varepsilon < 0. \quad (37)$$

In the intermediate time window, $1/\nu \ll t \ll t_\sigma$, the power laws identified for the memory kernel, $m(q, t) \sim t^x$ with $0 < x < 1$, result in power laws $\delta r^2(t) \sim t^x$. We get

$$\delta r^2(t) \sim \left(\frac{t}{\tau}\right)^x, \quad (38)$$

an intermediate window of anomalous power-law diffusion, with exponents $x = 1/2$ in the large- δ case, and $x = 2/3$ in the case of small δ .

Figure 8 exemplifies the behavior for $\delta = 10^{-3}$, corresponding to the memory kernels shown in Fig. 7. As stated above, the results are for overdamped Brownian dynamics; this version of Eq. (35) reads $\delta r^2(z) = (6/z^2)/[i\nu + m(0, z)]$, and the relevant asymptotic results are obtained by replacing $v_{\text{th}}^2 = 1$ in Eqs. (36) to (38). Again, a time scale \bar{t}^* can be identified where the contributions from the two asymptotic solutions balance. As in Eq. (34), $\bar{t}^*/\tau \sim 1/\delta^3$, but the prefactors are different:

$$\bar{t}^* \approx \frac{2}{\pi} \left(\frac{2\sqrt{2}\Gamma(5/3)}{\pi} \right)^6 \frac{\tau}{\delta^3}. \quad (39)$$

Note that $\bar{t}^* \approx 10t^*$, as is verified by comparing the marked positions in Fig. 7 and 8.

Recall that depending on δ the connection between ε and σ changes. However, $|\sigma|t_\sigma = \tau/|\varepsilon|$, and $h_\delta(0)$ changes relatively weakly with δ , so that Eq. (37) yields the same diffusion law, $\delta r^2(t) = 6Dt$ irrespective of δ , with a diffusion coefficient $D \sim |\varepsilon|$. On the localized side of the transition, Eq. (36) yields $r_c \sim \varepsilon^{-1}$ for the small- δ case, but $r_c \sim \varepsilon^{-1/2}$ for the large- δ case.

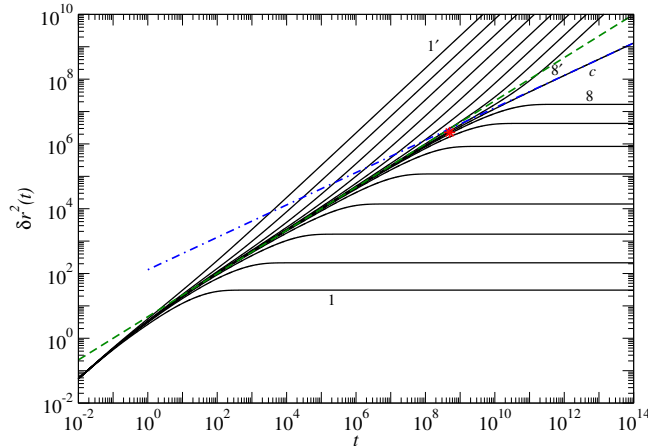


Figure 8. Mean-squared displacement $\delta r^2(t)$ vs. t for $\delta = 10^{-3}$ and various ε corresponding to the curves in Fig. 7. The anomalous-diffusion asymptote, $t^{1/2}$ ($t^{2/3}$) is shown as a dash-dotted (dotted) line. A star marks \bar{t}^* , Eq. (39).

4. Conclusions

We have discussed the different asymptotic regimes that emerge from MCT for the tagged-particle dynamics close to a localization transition, depending on an arbitrarily chosen infrared cutoff parameter δ . Such a parameter is not justified a priori, but can be rationalized by recognizing that the small- q structure of the MCT vertex for the LG case studied here is erroneous [28]. Reassuringly, in $d = 3$, the predicted position of the localization transition depends only weakly on δ , although its overall value suffers from similar disagreement with computer-simulation result as the MCT-predicted glass transition point. Note however that in $d = 2$ the situation changes. Following an argument of Ref. [46], one can show that the present MCT does not allow solutions recovering long-time diffusion if $\delta \rightarrow 0$; this results in a transition point that shifts to zero with decreasing δ . An analysis like the one presented here can still be carried through, if the changed structure of the vertex \tilde{v}_{qp} is taken into account [47].

Depending on the distance to the transition ε , and the cutoff δ , one observes power laws with different exponents for the memory kernel $m(q, t)$; one distinguishes the small- δ dynamics from the large- δ case, separated by a time scale t^* . This also holds for other dynamic quantities, like the mean-squared displacement $\delta r^2(t)$. The latter grows as $t^{1/2}$ for the large- δ case, which is the result also known from schematic MCT [27] and is the relevant result for previous numerical MCT calculations that do not treat the small- q anomalies of the vertex seriously. It is also, together with the $D \sim |\varepsilon|$ obtained above, the result expected from mean-field theory [48]. The results presented here also serve the purpose to highlight which parameter regimes can safely be treated by the present MCT in its widely used incarnation on a discrete wave-vector grid (where typically, $\delta \approx 0.2/R$), at least in $d = 3$.

Our introduction of a cutoff has analogies to a modern formulation of the renormalization group (RG) approach [49], where an infra-red cutoff controls the RG flow of the effective average action. It would be promising to establish an RG flow for the MCT equations, possibly following along the lines of a cluster-MCT [50], although it is not obvious how to do this.

Acknowledgments

This work was funded in part by the Deutsche Forschungsgemeinschaft, DFG, project P8 of the Research Unit FOR1394 “Nonlinear Response to Probe Vitrification”. Th. V. thanks for funding through the Helmholtz-Forschungsgemeinschaft (Impuls- und Vernetzungsfonds, VH-NG-406) and Zukunftskolleg, Universität Konstanz.

Appendix A. Numerical Procedure

We sketch the numerical scheme used to solve Eq. (10) and similar integral equations. To capture the behavior at small wave numbers, a logarithmic grid was introduced, containing N_s points starting at δ up to some Δq ; from Δq to an upper cutoff Q , N_Q equidistantly spaced points complete the grid. We used $N_s = 50$, $N_Q = 300$, $\Delta q = 0.08/R$, and $Q = 48/R$ for static calculations. Time-dependent quantities were obtained with $\Delta q = 0.4$ and $Q = 24/R$. These discretizations were found to be sufficiently accurate and have been checked with larger grids in some cases [47].

The critical eigenfunctions $h_\delta(q)$ and $\hat{h}_\delta(q)$ have been obtained by iteratively solving Eq. (10) starting with some constant initial guess; at each iteration step the approximate solution is inserted in the r.h.s., and the result is taken as the next approximant. As the iteration convergence is dominated by the eigenvalue ϱ_c , this procedure also determines the critical density, calculated as the ratio between the results of two iteration steps at fixed q .

For the time-dependent Eq. (3), a standard MCT algorithm is used where an equidistant grid is chosen for the time t , which is repeatedly coarsened by a factor 2 after a fixed number of steps in order to cover the required number of decades.

References

- [1] Kurzydum J, Coslovich D and Kahl G 2009 *Phys. Rev. Lett.* **103** 138303
- [2] Kim K, Miyazaki K and Saito S 2009 *EPL* **88** 36002
- [3] Höfling F, Franosch T and Frey E 2006 *Phys. Rev. Lett.* **96** 165901
- [4] Höfling F and Franosch T 2007 *Phys. Rev. Lett.* **98** 140601
- [5] Höfling F, Munk T, Frey E and Franosch T 2008 *J. Chem. Phys.* **128** 164517
- [6] Voigtmann Th and Horbach J 2009 *Phys. Rev. Lett.* **103** 205901
- [7] Moreno A J and Colmenero J 2006 *Phys. Rev. E* **74** 021409
- [8] Moreno A J and Colmenero J 2006 *J. Chem. Phys.* **125** 164507
- [9] Höfling F, Bamberg K U and Franosch T 2011 *Soft Matter* DOI:10.1039/C0SM00718H
- [10] Bunde A, Funke K and Ingram M D 1998 *Solid State Ionics* **105** 1–13
- [11] Voigtmann Th and Horbach J 2006 *Europhys. Lett.* **74** 459–465
- [12] Dingwell D B 1996 *Science* **273** 1054–1055
- [13] Voigtmann Th 2010 Multiple glasses in asymmetric binary hard spheres arXiv:1010.0440
- [14] Hajnal D, Brader J M and Schilling R 2009 *Phys. Rev. E* **80** 021503
- [15] Krakoviack V 2005 *Phys. Rev. Lett.* **94** 065703

- [16] Krakoviack V 2007 *Phys. Rev. E* **75** 031503
- [17] Krakoviack V 2009 *Phys. Rev. E* **79** 061501
- [18] Horbach J, Voigtmann Th, Höfling F and Franosch T 2010 *Eur. Phys. J. ST* **189** 141–145
- [19] Havlin S and Ben-Avraham D 2002 *Adv. Phys.* **51** 187
- [20] Kammerer A, Höfling F and Franosch T 2008 *EPL* 66002
- [21] Götze W 2009 *Complex Dynamics of Glass-Forming Liquids* (Oxford University Press)
- [22] Götze W and Voigtmann Th 2003 *Phys. Rev. E* **67** 021502
- [23] Franosch T and Götze W 1994 *J. Phys.: Condens. Matter* **6** 4807
- [24] Götze W, Leutheusser E and Yip S 1981 *Phys. Rev. A* **23** 2634–2643
- [25] Götze W, Leutheusser E and Yip S 1981 *Phys. Rev. A* **24** 1008–1015
- [26] Götze W, Leutheusser E and Yip S 1982 *Phys. Rev. A* **25** 533–539
- [27] Sjögren L 1986 *Phys. Rev. A* **33** 1254–1260
- [28] Leutheusser E 1983 *Phys. Rev. A* **28** 1762–1773
- [29] Resibois P and de Leener M 1977 *Classical Kinetic Theory of Fluids* (New York: Wiley & Sons)
- [30] Boon J P and Yip S 1980 *Molecular Hydrodynamics* (New York: McGraw-Hill)
- [31] Foffi G, Götze W, Sciortino F, Tartaglia P and Voigtmann Th 2003 *Phys. Rev. Lett.* **91** 085701
- [32] Franosch T, Höfling F, Bauer T and Frey E 2010 *Chem. Phys.* **375** 540–547
- [33] Franosch T and Voigtmann Th 2002 *J. Stat. Phys.* **109** 237–259
- [34] Götze W and Mayr M R 2000 *Phys. Rev. E* **61** 587–606
- [35] Götze W and Sjögren L 1995 *J. Math. Analysis Appl.* **195** 230–250
- [36] Götze W, Singh A P and Voigtmann Th 2000 *Phys. Rev. E* **61** 6934–6949
- [37] Letz M, Schilling R and Latz A 2000 *Phys. Rev. E* **62** 5173–5178
- [38] Chong S H and Götze W 2002 *Phys. Rev. E* **65** 041503
- [39] Chong S H and Götze W 2002 *Phys. Rev. E* **65** 051201
- [40] Kämmerer S, Kob W and Schilling R 1997 *Phys. Rev. E* **56** 5450–5461
- [41] Chong S H, Moreno A J, Sciortino F and Kob W 2005 *Phys. Rev. Lett.* **94** 215701
- [42] Porter D and Stirling D S G 1990 *Integral equations* (Cambridge University Press)
- [43] Jentzsch R 1912 *J. reine angew. Math.* **141** 235–244
- [44] Gripenberg G, Londen S O and Staffans O 1990 *Volterra Integral and Functional Equations* (Cambridge University Press)
- [45] van Beijeren H 1982 *Rev. Mod. Phys.* **54** 195–234
- [46] Götze W, Prelovšek P and Wölfle P 1979 *Solid State Commun.* 369–373
- [47] Schnyder S K 2010 Analysis of transport processes in glass-forming fluids in mode-coupling theory. Diploma thesis, Universität Konstanz
- [48] Stauffer D and Aharony A 1994 *Introduction to Percolation Theory* revised 2nd ed (Taylor & Francis)
- [49] Berges J, Tetradis N and Wetterich C 2002 *Phys. Rep.* **363** 223–386
- [50] Kroy K, Cates M E and Poon W C K 2004 *Phys. Rev. Lett.* **92** 148302